

See discussions, stats, and author profiles for this publication at: <https://www.researchgate.net/publication/231397332>

# Phase Separation of Mixed-Composition Self-Assembled Monolayers into Nanometer Scale Molecular Domains

ARTICLE *in* THE JOURNAL OF PHYSICAL CHEMISTRY · AUGUST 1994

Impact Factor: 2.78 · DOI: 10.1021/j100082a040

---

CITATIONS

259

READS

83

---

## 5 AUTHORS, INCLUDING:



[Stephan J Stranick](#)

National Institute of Standards and Technology

71 PUBLICATIONS 1,967 CITATIONS

[SEE PROFILE](#)



[Atul N Parikh](#)

University of California, Davis

175 PUBLICATIONS 6,884 CITATIONS

[SEE PROFILE](#)



[David L Allara](#)

Pennsylvania State University

261 PUBLICATIONS 23,185 CITATIONS

[SEE PROFILE](#)



[Paul S Weiss](#)

University of California, Los Angeles

395 PUBLICATIONS 12,015 CITATIONS

[SEE PROFILE](#)

# Phase Separation of Mixed-Composition Self-Assembled Monolayers into Nanometer Scale Molecular Domains

S. J. Stranick,<sup>†</sup> A. N. Parikh,<sup>‡</sup> Y.-T. Tao,<sup>‡,§</sup> D. L. Allara,<sup>\*,†,‡</sup> and P. S. Weiss<sup>\*,†</sup>

Departments of Chemistry and Materials Science and Engineering, The Pennsylvania State University, University Park, Pennsylvania 16802

Received: April 21, 1994; In Final Form: May 20, 1994\*

Scanning tunneling microscopy has been used to demonstrate phase segregation in varied composition, two-component self-assembled monolayers on gold. These monolayer films were assembled using  $\text{CH}_3(\text{CH}_2)_{15}\text{SH}$  and  $\text{CH}_3\text{O}_2\text{C}(\text{CH}_2)_{15}\text{SH}$ , two similar alkanethiol molecules which are non-hydrogen-bonding and have identical alkyl chain lengths. X-ray photoelectron spectroscopy, infrared spectroscopy, and ellipsometry have been used to characterize the average chemical compositions and average molecular structures of these films. Scanning tunneling microscopy of single composition, self-assembled monolayers of each of these molecules shows a preponderance of defects which can be attributed to single missing chains. In mixed composition films, we observe nanometer scale molecular domains with time-dependent shapes. These observations have important implications both for the fundamental understanding of solubilities and phase segregation in quasi-two-dimensional mixtures and for applications of self-assembly in which spatial patterns of adsorbate mixtures are important.

## I. Introduction

Self-assembled monolayers (SAMs) are being intensively studied because their well-defined structural character provides molecular surfaces of great promise for scientific studies and technological exploration. In particular, the ability to control the precise placement of selected functional groups on a flexible, substrate-bound molecular assembly will provide a means to replicate the physicochemical functions of biological surfaces and membranes.<sup>1</sup> In this regard, recent studies have shown that changes in the nature of functional groups exposed at SAM surfaces can affect the growth of cells<sup>2</sup> and the adsorption of proteins and other macromolecules.<sup>3</sup> Strategies for creation of complex, multifunctional surface architectures, such as in artificial receptor and other molecular recognition sites,<sup>4</sup> will require manipulation of exposed functional groups on the 1–100-nm scale. Developing such strategies requires a quantitative understanding of the intrinsic phase behavior of mixed monolayers. In particular, one must understand the tendency of unlike molecules to phase segregate into preferred spatial patterns on the nanometer scale in order to assess the stability of preformed patterns. At present, there does not appear to be any general understanding of these phenomena.<sup>5</sup> In order to achieve this understanding, reliable experimental methods are needed for characterizing the spatial distribution of molecules on the 1–100-nm scale. Due in large part to a lack of independent evidence to the contrary, homogeneous mixing has been routinely assumed for mixtures of terminally substituted alkanethiolates on gold, and subsequently, contact angle wetting data have been interpreted on this basis.<sup>6</sup> According to theoretical estimates, contact angle wetting methods would resolve domains no smaller than 0.1–1  $\mu\text{m}$ ,<sup>9</sup> so even “large” domains on the nanometer scale would produce the same wetting behavior as uniform mixing. In a recent study,<sup>10</sup> infrared spectroscopy has been used to infer that complete mixing occurs for 1:1 mixtures in two-component  $\text{CH}_3$ - and  $\text{HO}$ -terminated alkanethiolate monolayers on Au. One of the premier techniques for chemical imaging is time-of-flight secondary ion mass

spectroscopy (TOF-SIMS), but the current lateral resolution is limited to no smaller than  $\sim 50$  nm (the size of the ion beam spot).<sup>11</sup>

Scanning probe microscopies have sufficient lateral resolution and therefore appear the most promising for direct imaging of nanometer scale molecular patterns. Their use to date in studying organic films has been almost exclusively limited to non-chemically selective, topographical characterizations. In an encouraging application of atomic force microscopy (AFM), it has recently been shown<sup>7</sup> that phase-separated domains can be observed in Langmuir–Blodgett films formed by deposition from a mixture of an alcanoic acid and a partially fluorinated alkyl ether with a terminal carboxylic acid group, distinctly different molecules<sup>12</sup> with different lengths and functionalities. In the latter study,<sup>7</sup> the desired contrast was obtained using frictional response. There is as yet no indication of how general this technique will be, particularly since the frictional properties of various functional groups are not well understood. The tendency of mixed composition SAMs of distinctly different chain length alkanethiolates to phase segregate on gold has been inferred.<sup>13</sup> Monte Carlo simulations support such phase segregation.<sup>14</sup>

Based on the above discussion, the results presented in this study intersect the field at the point at which it appears that no general method has been demonstrated for distinguishing molecular patterns on surfaces on the nanometer scale and no understanding has been put forward to show what limits can be expected in the relationship between molecular similarity and phase segregation in quasi-two-dimensional systems.

In order to explore the possibilities of phase segregation near the limits of expected molecular compatibility, we have deliberately selected a pair of molecules of very similar size, very similar intermolecular interactions, and very similar terminal functional groups. These are  $\text{X}-(\text{CH}_2)_{15}\text{SH}$ , where  $\text{X}$  is  $\text{CH}_3$ - or  $\text{CH}_3\text{O}_2\text{C}-$ , alkanethiols of identical alkyl chain length where the only difference is the substitution of the terminal methyl group for a methyl ester group. A plethora of evidence has shown that the methyl group in  $\text{CH}_3(\text{CH}_2)_{15}\text{SH}$  is the outermost group.<sup>15</sup> Infrared spectroscopic evidence also suggests that for  $\text{CH}_3\text{O}_2\text{C}(\text{CH}_2)_{15}\text{SH}$  the methyl group is the outermost group exposed at the surface.<sup>16</sup> Despite these similarities, we show that these two thiolate molecules phase separate under ambient conditions into nanometer scale domains. These observations have important implications both for the scientific understanding of phase

\* To whom correspondence should be addressed.

<sup>†</sup> Department of Chemistry.

<sup>‡</sup> Department of Materials Science and Engineering.

<sup>§</sup> Permanent address: Academia Sinica, Institute of Chemistry, Nankang, Taipei, Republic of China.

• Abstract published in *Advance ACS Abstracts*, July 1, 1994.

segregation in quasi-two-dimensional molecular mixtures and for applications of self-assembly in which the formation of spatially resolved mixed functional group surfaces is *desired*. Further, these observations provide a caveat with regard to the common assumption of complete mixing in multicomponent self-assembled monolayers.

## II. Experimental Section

**II.A. Sample Preparation.** Substrates for STM studies were prepared by resistive evaporation of gold (99.999%) onto the surface of freshly cleaved mica which was preheated in vacuum to  $\sim 340$  °C.<sup>17</sup> The base pressure in the chamber during evaporation was  $\leq 6 \times 10^{-7}$  Torr. After  $\sim 100$  nm of gold was deposited, the substrate temperature was returned to  $<40$  °C while still under vacuum, then the chamber was back-filled with purified nitrogen, and the substrates were removed and immersed immediately in the thiol solutions (described below). Companion substrates were prepared by evaporating  $\sim 9$  nm of chromium followed by  $\sim 200$  nm of gold onto cleaned surfaces of polished, native oxide-covered single crystal Si(100) wafers according to a previously reported procedure.<sup>18</sup> The silicon wafer surfaces were precleaned by immersing the samples in a 1:4 mixture of  $\text{H}_2\text{O}_2/\text{H}_2\text{SO}_4$  at 110 °C for 10–15 min (*Warning: this solution reacts strongly with organic compounds and should not be stored in closed containers. It must be handled with extreme caution.*), followed by rinses in deionized purified water<sup>19</sup> and absolute ethanol. The freshly prepared Au/Cr/SiO<sub>2</sub>/Si samples were immediately characterized using single wavelength ellipsometry and then immersed directly (maximum ambient exposure of 5 min) into ethanolic solutions of  $\text{CH}_3(\text{CH}_2)_{15}\text{SH}$  and  $\text{CH}_3\text{O}_2\text{C}(\text{CH}_2)_{15}\text{SH}$  at 1 mM total thiol concentration. Four solutions were used: one pure solution of each thiol and two mixed solutions using 1:3 and 3:1 molar ratios of the two thiols. At these concentrations, both thiols are soluble in ethanol and readily form homogeneous solutions. The substrates were kept immersed in the solutions for 4 days at room temperature, after which the samples were withdrawn, rinsed in ethanol, and dried under a stream of nitrogen. Mica-supported samples were analyzed using STM. The companion samples were then characterized by X-ray photoelectron spectroscopy (XPS), ellipsometry, and infrared spectroscopy (IRS) to verify the quality, thickness, and composition of the assembled films.<sup>16,20</sup> The films were observed to be stable in air for the duration of the experiments. Neither XPS nor IR showed any evidence for the formation of sulfonates or other degradation products.

**II.B. Ellipsometry.** Ellipsometry measurements were recorded at a single wavelength (He–Ne laser, 632.8 nm) using a null ellipsometer<sup>21</sup> operating at a 70° angle of incidence. The measurement protocol for each sample involved the sequential measurement of the polarization parameters,  $\Delta$  and  $\Psi$  (directly related to polarizer and analyzer angles), at three arbitrarily chosen spots on each sample for freshly cleaned gold substrates and subsequently the thiolated substrates. The values of  $\Delta$  and  $\Psi$  then were translated into equivalent optical thicknesses using a standard three-phase model with sharp, planar interfaces.<sup>22</sup> The calculations utilized the pseudooptical functions of the freshly evaporated gold substrates, derived from their  $\Delta$  and  $\Psi$  values using a two-phase model, and a value of  $1.50 + 0i$  assumed for the complex optical constant of the thiolate films.<sup>23,24</sup> The spot-to-spot standard deviation on each sample was under 1 Å. The extreme sample-to-sample variations were within  $\pm 1$  Å, and averaging over multiple experiments gave standard deviations of  $\sim 0.5$  Å.

**II.C. Infrared Spectroscopy.** Infrared external reflection spectra were collected using an air ( $\text{CO}_2$ - and  $\text{H}_2\text{O}$ -free)-purged, custom-modified Fourier transform infrared spectrometer.<sup>25</sup> For quantitative spectra,<sup>26</sup> the incoming infrared radiation was focused onto the sample with an  $\sim f/20$  beam at an 86° angle of incidence, and the reflected beam was detected using a narrow-band HgCdTe

detector cooled with liquid nitrogen. A wire-grid polarizer was placed immediately before the sample and oriented to give p-polarization. The spectra were obtained using a mirror stroke amplitude set for 2-cm<sup>-1</sup> resolution with a data collection rate of 10 kHz. The interferograms were computed with triangular apodization and zero filling to provide accurate interpolation of peak frequency locations to 0.2 cm<sup>-1</sup>,<sup>26</sup> however, we more conservatively estimate accuracies to be 0.5 cm<sup>-1</sup>. The spectral intensities are reported as reflectivities in absorption units,  $-\log(R/R_0)$  where  $R_0$  is the reflectivity of a reference sample prepared by freshly cleaning an evaporated gold substrate using a UV-ozone cleaner.<sup>27,28</sup>

**II.D. X-ray Photoelectron Spectroscopy.** The XPS measurements were carried out with an in-house modified spectrometer<sup>29</sup> using monochromatized Al K $\alpha$  radiation (1486.6 eV) and a multichannel resistive anode detector and operating at a base pressure of  $\sim 1 \times 10^{-9}$  Torr. All analyses were conducted with a fixed photoelectron exit angle of 38.5° with respect to the surface normal. The resolution was determined from the full width at half-maximum of the Au4f<sub>(7/2)</sub> line to be 0.8–0.9 eV. No sample damage from X-ray exposure (typically 600-W power) was noted during the time required for the analyses. The compositions of the mixed monolayers were determined using the ratios of integrated counts of the O 1s and Au 4f<sub>7/2</sub> lines. This method is based on a variation of a previously reported procedure.<sup>30</sup> The typical error in the fractional compositions is estimated to be  $\pm 0.03$ .

**II.E. Scanning Tunneling Microscopy.** The STM images were recorded in air using a microwave-frequency-compatible beetle-style scanning tunneling microscope.<sup>31</sup> All the samples studied were sufficiently conductive that we were able to use dc tunneling current to control the tip–sample separation. All images were recorded at relatively large tunneling gap impedances,  $10^9 \Omega$ , to ensure large tip–sample separation. By measuring the tunneling current vs tip–sample separation all the way in to point contact with the underlying Au substrate, we have shown that the tunneling conditions used correspond to the tip being farther from the Au substrate than the outermost portion of the alkanethiolate layer.<sup>32</sup> In this way, we minimize the perturbation of the film by imaging with the probe tip out of contact with the film. All images were recorded in constant tunneling current mode and are presented unfiltered. STM piezoelectric scanner calibrations are performed by recording atomic resolution images of surfaces of known crystallography.

The means by which nominally insulating organic films can be imaged remains an important question in STM studies of these layers. Dürig *et al.* have conducted experiments on SAMs of HO(CH<sub>2</sub>)<sub>16</sub>SH on gold in which simultaneous STM and AFM images were recorded.<sup>34</sup> They showed that, in ultrahigh vacuum for tunneling gap impedances comparable to those used here ( $10^9 \Omega$ ), there was still apparently contact between the tunneling tip and the outermost region of the SAM. While Dürig *et al.* concluded that the pressure induced by the probe tip must play an important role in the ability of electrons to tunnel through the SAM, we note that tunneling can be assisted by the presence of “insulating” adsorbates in the STM tunnel junction even in the absence of contact.<sup>35</sup>

## III. Characterization of the Average Film Structure

The measured ellipsometric thicknesses of the series of films are shown in Table 1 as a function of the film compositions. Nuzzo *et al.* have reported values scattered around 22 Å for a series of terminally substituted X(CH<sub>2</sub>)<sub>15</sub>S chains on Au(111) surfaces, including X = CH<sub>3</sub> and CO<sub>2</sub>CH<sub>3</sub> substituents.<sup>16</sup> The methyl ester-substituted chains tended toward thicknesses of 24 Å.<sup>16</sup> A recent spectroscopic ellipsometry study has a best fit of 20.6 Å for the pure methyl-terminated film.<sup>23</sup> Examination of the data in Table 1 reveals that the present thickness values increase monotonically from 20.4 to 23.1 Å as the fraction of

**TABLE 1: Summary of the Observed Values of the Compositions, Ellipsometric Thicknesses, and the C-H Stretching Mode Frequencies for the Mixed Composition Methyl/Methyl Ester Monolayer Series**

solution	fraction of methyl ester component			film ellipsometric thickness ( $\pm 1 \text{ \AA}$ ) <sup>d</sup>	CH <sub>2</sub> group C-H stretching mode frequency ( $\pm 0.5 \text{ cm}^{-1}$ )	
	XPS <sup>a</sup> ( $\pm 0.03$ )	IR <sup>b</sup> ( $\pm 0.05$ )	STM <sup>c</sup> ( $\pm 0.04$ )		symmetric	antisymmetric
0.0	0.0	0.0	0.0	20.4	2850.2	2917.8
0.25	0.21	0.29	0.24	20.7	2850.3	2918.5
0.75	0.61	0.67	0.73	21.9	2850.3	2918.7
1.0	1.0	1.0	1.0	23.1	2850.8	2918.8

<sup>a</sup> Determined from the O (1s)/Au(4f<sub>7/2</sub>) XPS peak areas (see text). <sup>b</sup> Determined from the relative peak areas of the 2878-cm<sup>-1</sup> C-H stretching mode of the CH<sub>3</sub> group of the hexadecanethiolate adsorbate (see text). <sup>c</sup> Determined from the averaged ratios of the domain areas measured in multiple STM images (see text). <sup>d</sup> Sample-to-sample variation (see text).

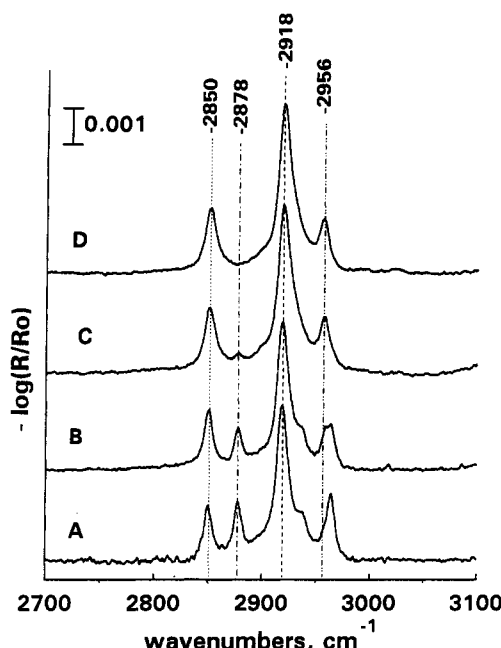


**Figure 1.** Infrared spectra of the pure and mixed self-assembled monolayer films for ratios of  $\text{CH}_3(\text{CH}_2)_{15}\text{SH}$  to  $\text{CH}_3\text{O}_2\text{C}(\text{CH}_2)_{15}\text{SH}$  on Au of (A) 1:0, (B) 3:1, (C) 1:3, and (D) 0:1. The integrated intensity of the symmetric methyl stretching mode absorption at 2878 cm<sup>-1</sup>, present only for the methyl-terminated thiol, is used to determine the fraction of the surface covered by  $\text{CH}_3(\text{CH}_2)_{15}\text{SH}$ .

methyl ester-terminated thiolate component increases, in good agreement with the previous work.<sup>16</sup> Although the thickness values observed in this study vary up to  $\pm 1 \text{ \AA}$  from sample to sample, the difference from pure CH<sub>3</sub> to pure CO<sub>2</sub>CH<sub>3</sub>-terminated thiolate films appears outside of this error and implies that there is a one to several angstroms difference in the film thicknesses between the two pure composition films. Space-filling models of fully extended chains show a difference in length of  $\sim 1\text{--}2 \text{ \AA}$  with the exact value set by the specific conformation of the methyl ester group. This difference in length will translate into a difference in film thickness according to the tilt of the angles of the chains. Previous studies indicate that the *n*-alkanethiolate chains are tilted on average  $\sim 26\text{--}30^\circ$ ,<sup>20,36</sup> while recent studies have set the average tilts of the methyl ester chains at 30–34°.<sup>37</sup> On the basis of the average of these tilt angles ( $\sim 30^\circ$ ), the two monocomponent films should show a difference of 1–2 Å with the exact value dependent upon the conformation of the ester group. For higher precision data, other approaches such as spectroscopic ellipsometry combined with accurate modeling are required.<sup>23</sup>

Figure 1 shows the infrared reflection spectra in the C-H stretching mode region of the four self-assembled monolayer compositions referred to in Table 1. The CH<sub>2</sub> symmetric and antisymmetric stretching mode absorptions are observed at nearly composition-independent values of 2850–2851 and 2918  $\pm 0.5 \text{ cm}^{-1}$ , respectively. Previously reported values of these peak frequencies for the pure methyl ester-terminated films are 2852 and 2918 cm<sup>-1</sup>,<sup>16</sup> and for the pure methyl-terminated films are

2850 and 2918 cm<sup>-1</sup>,<sup>20</sup> in good agreement with the present data which have been analyzed with higher precision than previously. It can be concluded, based on the positions of these peaks, that these spectra arise from film structures consisting of densely packed assemblies of alkyl chains in predominantly *all-trans* conformations.<sup>38</sup> The complete assignment of the C-H stretching mode spectral features of the single composition monolayers has been made elsewhere,<sup>16,20</sup> therefore, it will not be dealt with here except for the symmetric CH<sub>3</sub> stretching mode at  $\sim 2878 \text{ cm}^{-1}$  which is discussed below. A complete vibrational analysis of the compositional effects on the spectra, including the lower frequency modes (below 2000 cm<sup>-1</sup>), confirms the above structural conclusions and reveals additional details of vibrationally sensitive structural features, such as reorientation of the CO<sub>2</sub>CH<sub>3</sub> group at low ester fractions (<25%).<sup>37</sup>

The primary determination of the film compositions was done by analysis of the XPS data. The XPS spectra of the C 1s, O 1s, and S 2p core levels of the two monocomponent films are identical in terms of the spectral shapes to those reported earlier<sup>20</sup> and are not shown here as little new can be added to the previous analyses. The spectra of the mixed composition films change uniformly with composition as would be expected for a linear averaging of the two components in the observed spectra. Table 1 presents the XPS-derived compositions (details are given in section II) as a function of the ethanolic solution composition for the two compositions investigated by STM. The film compositions reflect the solution mole fractions in that surface composition depends monotonically on solution composition. However, the relationship deviates from linearity as the ester concentration increases. In order to provide a more thorough evaluation of the film composition, an independent measurement was made using the symmetric C-H stretching mode absorption peak of the terminal CH<sub>3</sub> group in the hexadecanethiolate chain. This feature appears at  $\sim 2878 \text{ cm}^{-1}$  (Figure 1) and diminishes in intensity with decreasing CH<sub>3</sub> and increasing CO<sub>2</sub>CH<sub>3</sub> content. The intensity of this absorption will depend upon the surface concentration of this species, the orientation of the CH<sub>3</sub> group (more rigorously, the transition dipole moment of the mode), and the intrinsic value of the absorption coefficient of the mode. Since there appears to be no change in the chain alignments across the composition series, as judged from the other modes of the IR spectra (see Table 1), the alkyl CH<sub>3</sub> group orientation can be assumed to be constant. Further, since the frequency of the mode is composition independent (see Figure 1), which indicates that the force constant associated with the normal mode is constant, it is quite reasonable to assume that the absorption coefficient, which is controlled by the charge flow (dynamic dipole) during vibration, is constant. On this basis, the integrated absorption due to this peak therefore can be used as a basis to estimate the film compositions. The results are given in Table 1 and are in agreement with the XPS-derived values.

#### IV. Single-Component Self-Assembled Monolayers

We have recorded many hundreds of images of single composition self-assembled monolayers of  $\text{CH}_3(\text{CH}_2)_{15}\text{SH}$  and  $\text{CH}_3\text{O}_2\text{C}(\text{CH}_2)_{15}\text{SH}$  on Au. Representative examples are given

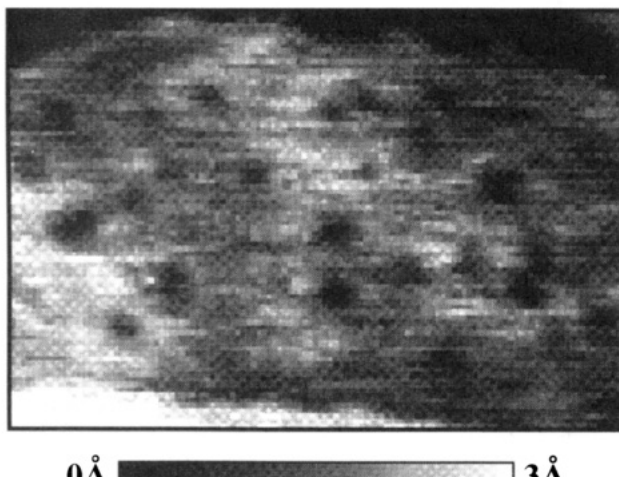


**Figure 2.** A scanning tunneling microscope image showing a  $440 \times 300$  Å<sup>2</sup> area of a self-assembled monolayer of  $\text{CH}_3(\text{CH}_2)_{15}\text{SH}$  on Au. The image was recorded in constant-current mode at a tunneling current of 2 nA and a tip bias voltage of -2 V. The area imaged includes a monatomic height step in the Au substrate. All images show unfiltered data.

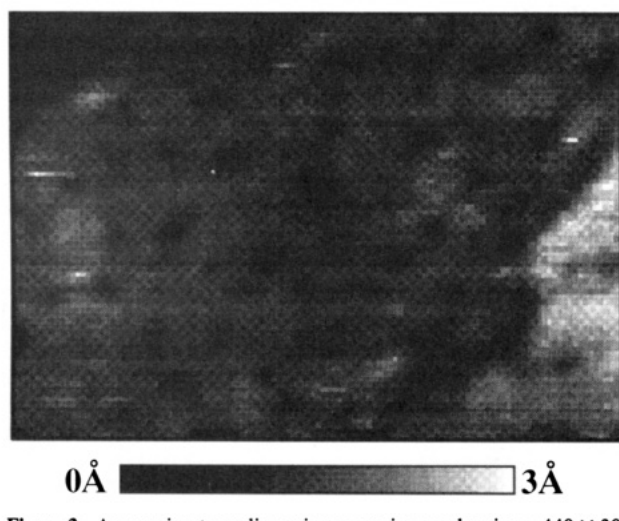


**Figure 3.** A scanning tunneling microscope image showing a  $440 \times 300$  Å<sup>2</sup> area of a self-assembled monolayer of  $\text{CH}_3\text{O}_2\text{C}(\text{CH}_2)_{15}\text{SH}$  on Au. The image was recorded in constant-current mode at a tunneling current of 2 nA and a tip bias voltage of -2 V. The area imaged includes a monatomic height step in the Au substrate.

in Figures 2 and 3 which show flat, featureless regions populated by small areal fractions of uniform size defects, observed as dark spots. The characteristics of these images match the best literature examples with respect to atomic flatness and defect densities.<sup>34,39,40</sup> The defects are observed in detail as depressions of ~1-Å depth by 20–25-Å diameter. Further, under the present tunneling conditions, both the positions and the dimensions of these defects are stable with respect to repeated STM imaging. We note that depressions have been observed in previous STM studies of alkanethiolate/Au monolayers and that the identification of these defects remains a subject of current controversy.<sup>34,39–42</sup> Similar size defect features have been noted in *n*-alkanethiolate SAMs by Edinger *et al.*<sup>39</sup> and McCarley *et al.*,<sup>42</sup> who both attributed these defects to etching of substrate gold atoms during monolayer adsorption. Schönenberger *et al.* have resolved individual molecules of self-assembled monolayers of  $\text{CH}_3(\text{CH}_2)_{n-1}\text{SH}$  on Au{111}, where  $n = 12$ .<sup>43</sup> Poirier and Tarlov have done the same for shorter chain alkanethiolate ( $n = 4, 6, 8$ ) monocomposition SAMs on Au{111} in ultrahigh vacuum.<sup>44</sup> Both groups observed defects larger laterally and at higher density than those found here. In each case, these were convincingly shown to be due to one atom deep pits in the underlying Au substrate covered with the alkanethiolate SAM.<sup>43,44</sup> Their images were recorded at high tunneling gap impedance. Poirier and Tarlov found that their

defects were stable for days in ultrahigh vacuum.<sup>44</sup> Similarly, Porter and co-workers have imaged the  $(\sqrt{3} \times \sqrt{3})R30^\circ$  alkanethiolate structure within one Au atom deep pits in the alkanethiolate-covered Au{111} surface.<sup>45</sup> Dürig *et al.* have examined SAMs of  $\text{HO}(\text{CH}_2)_{16}\text{SH}$  on Au and observed 30–50-Å-diameter depressions,  $2.5 \pm 0.5$  Å deep, which moved under the influence of the STM tip and combined to make larger defects.<sup>34</sup> Dürig *et al.* attributed these features to *gauche* defects in the alkyl chains.<sup>34</sup>

The origin and detailed nature of the defects in the present study cannot be determined from the STM images alone. One reason for this situation is that the feature heights in STM images do not give a true topographic height measurement since the tunneling probability is a convolution of the geometric and electronic surface structure.<sup>35</sup> However, it does appear that the defects observed in Figures 2 and 3 are inherently different than those reported by Dürig *et al.* on the basis that the latter are significantly larger than the present ones and move under the influence of the STM probe tip under similar tunneling conditions. The point defects here are also different than those found in refs 43 and 44 on the basis of their size and shape. One type of defect that can be expected in SAMs, of all types and on all substrates, is a region of missing adsorbate. In line with this, at ~25 times shorter monolayer formation times than used for the monolayers imaged in Figures 2 and 3, 4 h (vs 100 h), we observe increased defect dimensions, 70–100-Å-diameter regions of ~4–8-Å depth, in reasonable agreement with the report of Kim and Bard<sup>40</sup> for preparation under similar short times and conditions. These defect features may be attributed to regions of the bare gold surface which become smaller in diameter with increasing incubation times in the thiol solutions. In this picture, the free volume available, *viz.*, equivalent to that of the missing chains, would provide a space for thermally driven relaxation of the surrounding chains via conformational isomerization with a resulting redistribution of chain segment density into a dish or bowl shape with gradually sloping edges and, for small numbers of missing chains, a depth which is less than the total film thickness, consistent with what is observed in Figures 2 and 3 for our films.<sup>46,47</sup> Further, regions of multiple missing adsorbate chains may be expected to show some mobility with respect to the influence of the tip since bare substrate areas provide open sites for adsorbate translation as well as space for chain segment motion via conformational isomerization. At our long incubation times it is reasonable to expect that the sizes of these missing chain defects would approach those due to single missing chains with a corresponding approach to limiting defect attributes, of which two are relevant to our observations. First, since this missing chain volume is a minimum value, *viz.*, one chain, there will be an associated minimum in the number of possible conformations accessible for the relaxing neighboring chains with a resultant minimum in any tip-induced deformation of the defect region, relative to defects with larger numbers of missing chains. Since the defects observed by Dürig *et al.*<sup>34,48</sup> are up to twice the diameter of the typical ones observed in the present work (Figures 2 and 3), it would follow that the stability of the present defects would be relatively higher with respect to tip-driven motion. In agreement with this picture, McCarley *et al.*<sup>42</sup> observe that, at lower tunneling impedances than our measurements (smaller tip-sample separations), substantially larger defects than those in Figures 2 and 3 are susceptible to tip-induced motion and coalescence. Second, the minimum bare substrate surface available in a single chain defect, *viz.*, one surface site, would render this limiting defect with a minimum mobility via a chain translation mechanism, in accordance with the lower mobility of the defects shown in Figures 2 and 3 relative to those reported by Dürig *et al.*<sup>34</sup> and McCarley *et al.*<sup>42</sup> At high tunneling gap impedance and nearly full surface coverage, the STM tip would not be expected to move the missing Au defects as found by Poirier and Tarlov.<sup>44</sup>

In summary, with sufficiently long incubation periods for the film formation, the preponderant defects we observe are immobile



**Figure 4.** A scanning tunneling microscope image showing a  $440 \times 410 \text{ \AA}^2$  area of a self-assembled monolayer of a mixture of 25%  $\text{CH}_3(\text{CH}_2)_{15}\text{SH}$  and 75%  $\text{CH}_3\text{O}_2\text{C}(\text{CH}_2)_{15}\text{SH}$ . The gray scale and tunneling conditions are the same as in Figures 2 and 3. By comparison with images such as the one shown in Figure 5, we infer that the regions that appear higher in the image (brighter) are  $\text{CH}_3\text{O}_2\text{C}(\text{CH}_2)_{15}\text{SH}$  domains and the regions that appear lower (darker) are  $\text{CH}_3(\text{CH}_2)_{15}\text{SH}$  domains.

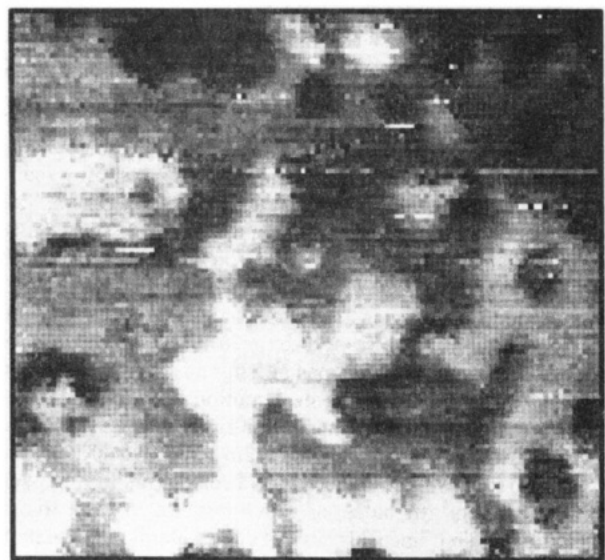


**Figure 5.** A scanning tunneling microscope image showing a  $440 \times 410 \text{ \AA}^2$  area of a self-assembled monolayer of a mixture of 75%  $\text{CH}_3(\text{CH}_2)_{15}\text{SH}$  and 25%  $\text{CH}_3\text{O}_2\text{C}(\text{CH}_2)_{15}\text{SH}$  on Au. The gray scale and tunneling conditions are the same as in Figures 2 and 3. By comparison with images such as the ones shown in Figures 4 and 6, we infer the identity of the molecules in the domains as described in the caption to Figure 4 and in the text.

and appear  $\sim 1 \text{ \AA}$  deep and  $20\text{--}25 \text{ \AA}$  across. These are the smallest and by far the most common defects that appear in the STM images of the *single*-component thiolate monolayers on Au{111} terraces. The distribution and further characterization of these defects will be the topic of a future publication.<sup>46</sup> The identification and properties of these as well as the larger defects found for these remain controversial. Here we use these defects as a marker of one of the properties of single-component SAMs.

## V. Two-Component Self-Assembled Monolayers

Figures 4 and 5 show representative constant-current images of nominal 1:3 and 3:1 mixed monolayers of  $\text{CH}_3(\text{CH}_2)_{15}\text{SH}$  and  $\text{CH}_3\text{O}_2\text{C}(\text{CH}_2)_{15}\text{SH}$ , respectively. Again, as with the mono-composition films, hundreds of images were recorded over different

surface regions with multiple samples, and the images shown are representative in terms of the shapes, sizes, and stabilities of the features. The data shown in the figures are the first images taken over previously unexamined regions of the SAM surfaces. Further, the tunneling conditions remained identical for both the imaging of the single- and mixed-composition SAMs. Figure 6a also shows a constant-current image of a 1:3 mixed monolayer of  $\text{CH}_3(\text{CH}_2)_{15}\text{SH}$  and  $\text{CH}_3\text{O}_2\text{C}(\text{CH}_2)_{15}\text{SH}$ , respectively, but uses a color scale to represent topographic information in order to highlight features shown in Figure 6b. Three major types of features are observed: (1) a preponderance of large, irregularly shaped regions which differ in height by  $\sim 1 \text{ \AA}$ , (2) a small fraction of  $\sim 1\text{-\AA}$  depressions of  $20\text{--}25\text{-\AA}$  diameter, quite similar to the defects observed in monocomposition films, and (3) a small fraction of  $\sim 5\text{--}7\text{-\AA}$ -diameter regions located in the middle of the larger regions and depressed  $\sim 1 \text{ \AA}$  below that surface,<sup>49</sup> defects unlike any observed in the monocomposition film images. We discuss these three features in order.

Two possibilities exist as the basis of the dominant, large features observed above: (1) defects related to the type observed in monocomposition films and (2) domains of pure alkanethiolate. Since these features are distinctly unlike any observed in the monocomposition SAM images<sup>50</sup> in terms of shapes, it seems unlikely that they are due to such causes as missing adsorbate chains. However, in order to distinguish between the above two possibilities more definitively, the fractional surface areas of these domains were analyzed to see if a correlation exists between these areas and the known SAM compositions. The analyses were conducted by recording the tip heights associated with each image pixel for a pixel size ( $2.8 \text{ \AA}$ )<sup>2</sup>. Examples of these data in histogram form are shown in Figure 7, a and b, where the full areas of the images shown in Figures 4 and 5, respectively, were analyzed. The plots show the number of pixels at various relative topographic heights found in the images. In the analysis, only the overall statistical populations of tip height readings which differ on average by  $\sim 1 \text{ \AA}$ , with no bias toward the specific location in the images, were determined, and no attempt was made to utilize the data for determination of individual feature areas. That is, in this analysis we have lost the information given by the topography of the neighboring pixels and surrounding region evident in the images of these mixed-composition films. The binning of the domains by topography was done according to the location of the dashed dividing lines in the histograms with no attempt to deconvolute peaks from these distributions. The dividing lines for the bins were chosen using the images—before the information intrinsic to the patterns formed by the domains was discarded. Noise in imaging puts some pixels well above and below the mean values for the domain. Analysis of the data in Figure 7a,b results in area ratios of 2.6:1 and 1:3.0 corresponding to the nominal 3:1 and 1:3 methyl ester- and methyl-terminated alkanethiolates, respectively. The measured compositions in Table 1 are averages of the analyses of several images at each SAM composition. These results indicate that the large features in Figures 4 and 5 correspond to domains of pure alkanethiolate and, further, show that the methyl ester-terminated SAM domains correspond to the  $\sim 1\text{-\AA}$  higher tip height regions. Although this distance correlates with the larger ellipsometric thickness of the pure ester-terminated SAM relative to the methyl-terminated one (section III), we caution that the exact connection between the tip heights and the topographic feature heights cannot be specified since it depends upon unknown details of the local density of states involved in the tunneling process in these constant-current images. The tip height changes in passing from one domain to another can be seen in detail in Figure 8a where a cross section is shown for the line marked (as A-A') in Figure 6b.

Figure 6a shows an image of a 1:3 methyl ester-, methyl-terminated SAM in which a single monocomposition type of defect is visible (as a blue spot) in the interior of a methyl domain (marked M' in Figure 6b). A tip height profile across this defect (B-B' in Figure 6b) is shown in Figure 8b where it is seen that

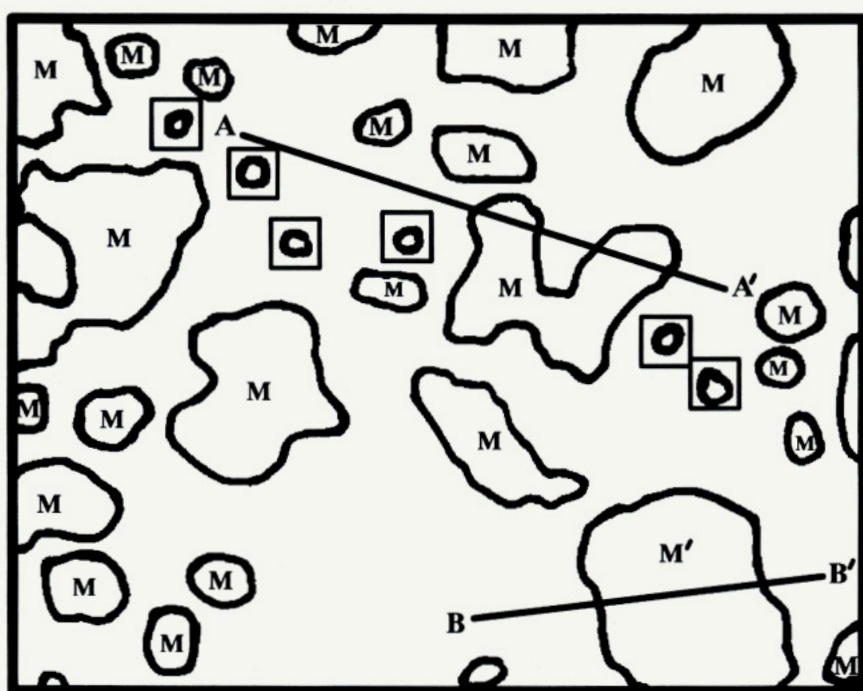
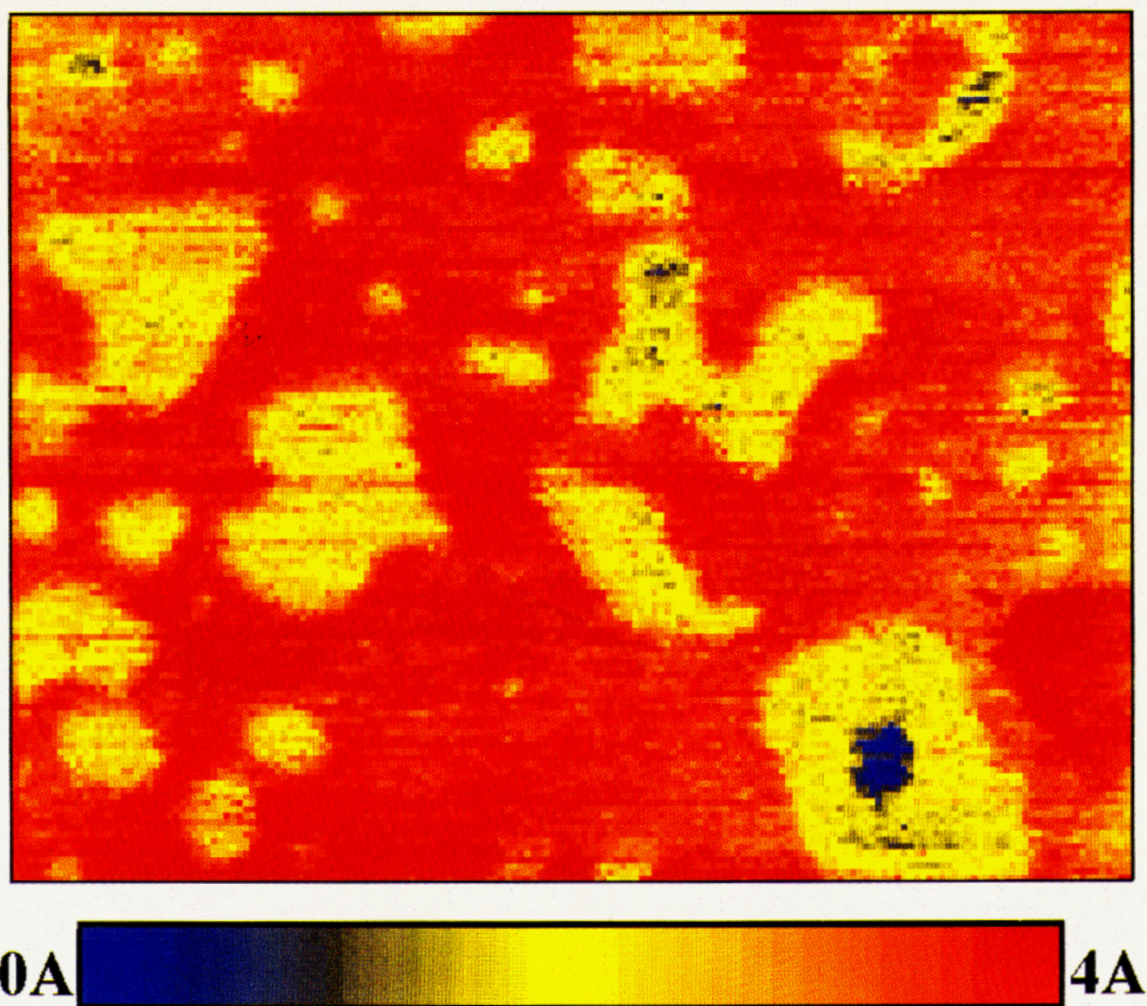


**Figure 6.** (a) A scanning tunneling microscope image showing a  $500 \times 390 \text{ \AA}^2$  area of a self-assembled monolayer of a mixture of 25%  $\text{CH}_3(\text{CH}_2)_{15}\text{SH}$  and 75%  $\text{CH}_3\text{O}_2\text{C}(\text{CH}_2)_{15}\text{SH}$  on Au. The tunneling conditions are the same as in Figure 4. Note the molecular void defect (blue) in the  $\text{CH}_3(\text{CH}_2)_{15}\text{SH}$  domain in the lower right area of the image. (b) A schematic of the image shown in (a). The domains attributed to the methyl-terminated thiolate are outlined and labeled by M. The region containing a molecular void defect is labeled M'. The single methyl-terminated molecule domains are enclosed in squares. The lines indicated by A-A' and B-B' show the line scans extracted to produce Figure 8.

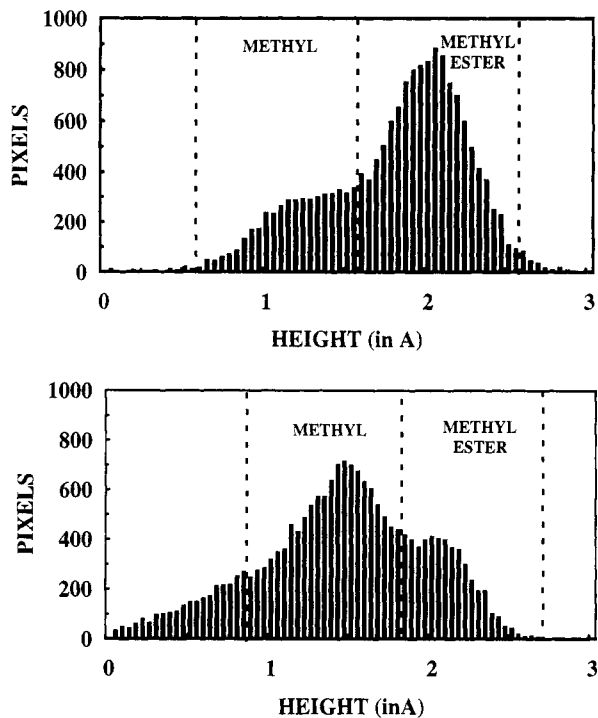


**Figure 7.** (a) Histogram of the topography of the STM image shown in Figure 4, a self-assembled monolayer of a mixture of 25%  $\text{CH}_3(\text{CH}_2)_{15}\text{-SH}$  and 75%  $\text{CH}_3\text{O}_2\text{C}(\text{CH}_2)_{15}\text{-SH}$ . The dashed lines indicate the positions used to delineate between the domains of the two molecules. This is used to determine the composition of the film in the area imaged. (b) Histogram of the topography of the STM image shown in Figure 5, a self-assembled monolayer of a mixture of 75%  $\text{CH}_3(\text{CH}_2)_{15}\text{-SH}$  and 25%  $\text{CH}_3\text{O}_2\text{C}(\text{CH}_2)_{15}\text{-SH}$ .

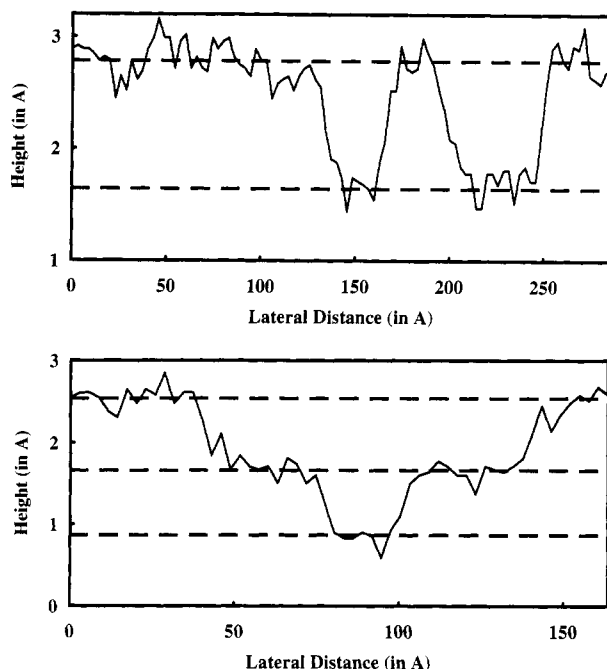


**Figure 8.** (a) Topography along a line scan from Figure 6a as indicated by the A-A' line in Figure 6b in order to show the height difference of the domains of the two thiolate molecules. The dashed lines indicate the average height of the molecular domains in the image. (b) Topography along a line scan from Figure 6a as indicated by the B-B' line in Figure 6b in order to show the height difference of the domains of the two thiolate molecules and the molecular void defect present in the methyl domain. The dashed lines indicate the average height of the molecular domains and of the molecular void defect in the image.

the methyl region in which the defect feature is located appears at an  $\sim 1 \text{ \AA}$  lower height than the surrounding methyl ester surface and that the defect, in turn, exhibits an  $\sim 1 \text{ \AA}$  deep by  $\sim 25 \text{ \AA}$  diameter profile typical of the monocomposition film defects

observed (Figures 2 and 3). The location of this defect feature at tip heights below the surfaces of both of the alkanethiolate domains is consistent with a missing adsorbate defect, as discussed above. Defects of this type in the methyl ester-terminated alkanethiolate domains are difficult to distinguish from domains of appropriately sized and shaped methyl-terminated alkanethiolate. Few of the domains meet these criteria. In our data analysis, defects in the methyl ester-terminated alkanethiolate domains would have the effect of reducing by a few percent the measured ratio of methyl ester- to methyl-terminated SAMs deduced from the STM images.

The smallest of the three types of features exhibit  $\sim 5\text{--}7\text{-\AA}$  diameters. Examples of these features located within a methyl ester-terminated alkanethiolate domain can be seen in Figures 6a,b (where they are identified by the boxed regions). These particular features are also  $\sim 1 \text{ \AA}$  deep. Repeated scans over the same areas gave reproducible images, and the features moved at rates of less than one hop per hour, essentially the same as the rates of molecular exchange observed to occur between larger domain boundaries (discussed in section VII). On the basis that the lateral interchain spacing for a  $(\sqrt{3} \times \sqrt{3})R30^\circ$  alkanethiolate monolayer on Au(111) is  $5.1 \text{ \AA}^{15,51}$  and that the tip heights for the methyl-terminated alkanethiolate domains are consistently  $\sim 1 \text{ \AA}$  lower than the methyl ester-terminated alkanethiolate domains, we tentatively assign these smallest features to single-molecule inclusions of methyl-terminated thiolate within domains of methyl ester-terminated thiolate.

The above observations and analyses demonstrate that the monolayers do not represent the limiting case of an ideal solution in which complete mixing occurs. This conclusion is in contrast to that which would be inferred from the approximate correspondence of the solution compositions and the film compositions, shown in Table 1. The STM data thus indicate that the self-interaction energies of each component are larger than the cross-interaction.<sup>55</sup> This would drive the phase segregation and also have the effect of creating an interface energy resulting in an "edge tension" (interface line tension) in these domains. From a very simple analysis this tendency for phase segregation seems surprising because the major intermolecular interactions would be expected to be dominated by  $\text{CH}_2\text{-CH}_2$  forces between the  $-(\text{CH}_2)_{15}-$  chain sections which should be nearly indistinguishable for any combination of the two alkanethiolate molecules in a film structure. However, it is apparent that contributions from the weakly polar  $-\text{CO}_2\text{CH}_3$  groups must be considered in realistic approximations of the interaction energetics. We discuss these points further in the sections below.

## VI. Mechanism of Domain Formation in Two-Component Monolayers

With regard to the origins of the formation of these domains, we consider three limiting scenarios. First, in the commonly assumed surface-collision-controlled (kinetic) limit, solute thiol molecules strike the surface randomly and adsorb irreversibly, immobilized on the surface. The result of this process would be a completely random statistical distribution of adsorbate molecules exactly reflecting the solution composition. Since domains are observed, this limiting mechanism cannot hold, and there must be a reflection of the equilibrium character in the film structures. There are two kinetic channels to enable such equilibrium character, *viz.*, surface diffusion and desorption. Second, in a surface-diffusion-limited mechanism, irreversible chemisorption would occur, followed by surface diffusion which (given sufficient time) would allow complete redistribution of the adsorbates to form their preferred spatial distributions. The overall compositions would be fixed by the kinetic constraints of the initial adsorption process. The film can then be considered a closed system, incapable of reaching equilibrium with the solution. Third, in a solution-interchange-limited mechanism, even with no surface mobility, adsorption-desorption processes would eventually lead

to the equilibrium structure of the film via solution exchange. A variety of intermediate mechanisms could result from combinations of these three cases (and others not considered here as well).

Folkers *et al.* have suggested that if solution exchange occurs readily for a mixed composition SAM of a long chain alkanethiol and a short chain alkanethiol (*i.e.*, the film is in equilibrium with the solution), the result is likely to be that the film will consist only of a single phase.<sup>56</sup> Various studies have shown that solution exchange is slow, and equilibration between solution and film is therefore difficult to obtain.<sup>56-58</sup>

Careful examination of the time dependence of the STM images in fully formed films (see section VII) demonstrates that some degree of surface mobility exists at room temperature. Regardless of the exact mechanism for the spatial redistribution of the adsorbates, it is clear that our observations of domain formation require that *some* fraction of the thermodynamic equilibrium character be reflected in the film formation process. Therefore, the true equilibrium structure must consist of discrete molecular domains on *some* size scale.

## VII. Motion of Alkanethiolates in Self-Assembled Monolayers

From the above discussion it is clear that surface diffusion can play an important role in domain formation. In order to investigate this aspect further, we have carried out time-dependent imaging of single- and mixed-composition monolayers and have examined the character of the diffusion both at substrate defects, such as step edges, and on large Au{111} terraces. In the discussion below, only diffusion on terraces is considered. The study of motion of the thiolate-covered Au{111} step edges is quite extensive and will be reported elsewhere.<sup>59</sup>

A number of precautions have been taken to ensure that the observed rates of motion are intrinsic and not dependent upon our imaging rate or repetition. In particular, the delay period between subsequent scans has been varied. During this delay period, we have positioned the STM tip at the center of the area imaged and at other positions to verify that no special rearrangement occurs in the vicinity of the tip as the tunneling parameters are maintained.<sup>60</sup>

In Figure 9, two consecutive images, taken 37 min apart, show a  $500 \times 390 \text{ \AA}^2$  region of the 25%  $\text{CH}_3(\text{CH}_2)_{15}\text{SH}$  and 75%  $\text{CH}_3\text{O}_2\text{C}(\text{CH}_2)_{15}\text{SH}$  SAM on a large terrace. The arrows indicate regions where adsorbate exchange has taken place. This is indicated by changes in the topographic height from values typical of  $\text{CH}_3\text{O}_2\text{C}(\text{CH}_2)_{15}\text{SH}$  (red) to values typical of  $\text{CH}_3(\text{CH}_2)_{15}\text{SH}$  (yellow), suggesting coalescence of initially isolated domains of  $\text{CH}_3(\text{CH}_2)_{15}\text{SH}$ . Importantly, we have never observed the reverse process in which a single domain of one thiolate breaks up into two or more domains. This slow rate of exchange is independent of the number of times an area has been scanned under these tunneling conditions, as noted above.

Two conclusions can be drawn from the observations of this thiolate exchange and coalescence. First, since the process is unidirectional with the domains growing by coalescence, it is apparent that the structure is not yet near local equilibrium. Second, since the thiolate molecules are able to move within the densely packed monolayer the only way in which space could be made available for adsorbate translation would be via concerted motion of other adsorbate molecules in the region. At present, we have no mechanistic model for this process.<sup>61</sup> While the motion of individual molecules would be driven by thermal fluctuations, we speculate that the overall flow governing domain redistribution would be driven by the thermodynamics of the edge tension of the quasi-two-dimensional domains. Both of the exchanges indicated in Figure 9 occur at points of high curvature within at least one of the domains, leading further credence to this argument. We note that we see the curvature of the domains reduce and the sizes of the domains increase over time periods of hours. We further note that the observed rates of the above exchange are

slow compared to the rates of  $\sim 10$  atoms per step site per hour, which we have observed to occur at step edges for pure *n*-alkanethiolate films.<sup>59</sup> Further evidence that the smallest features in the mixed-composition SAMs are due to single molecular inclusions (domains of single molecules as discussed in section V) comes from the observation that these domains move slowly via exchange within the film.

Finally, we point out that even though there is a finite mobility associated with these SAMs the values are quite low compared to those for Langmuir films (at the air-water interface). Such mobility differences should be reflected in differences in domain formation for the chemically bound SAMs and Langmuir films.<sup>5-7</sup>

## VIII. Effects of Gold Morphology on SAM Properties

The preceding STM results clearly define important aspects of the organization of alkanethiolate monolayers on Au{111} terraces. However, a typical gold surface, such as one prepared by vapor deposition, consists of both {111} terraces and mixed-morphology boundary regions containing steps, kinks, and other defects.<sup>18,62,63</sup> This morphology is expected to be important in determining the functional properties of SAMs on these substrates, particularly transport through the films such as occurs in electrochemistry at functionalized gold electrodes. With this in mind, we examine the results of this study in further detail with respect to the possible effects of morphology.

The results in Table 1 show that the solution compositions are reflected in the STM-determined surface compositions for Au{111} terraces. Two limiting models, kinetic and equilibrium, would be consistent with this observation: (1) chemisorption is irreversible (no desorption) with thiol solute molecules arriving at the surface at rates proportional to their solution concentrations, and (2) chemisorption is completely reversible (desorption allowed) with no preferred interactions between the two component thiols, *viz.*, ideal solution behavior. However, in view of the observed formation of domains, case 2 is eliminated. The lack of solution exchange implied by case 1 would be consistent with the relatively slow desorption rate expected for the strong Au–thiolate bond,  $\sim 44 \text{ kcal/mol}$ .<sup>15,64</sup> In addition, as coverages increase, further contributions to the desorption barriers arise due to increasing intermolecular interactions which approach energies of  $\sim 1.4\text{--}1.8 \text{ kcal/mol}$  per  $\text{CH}_2$  group in dense films.<sup>15</sup>

In contrast to the above behavior on {111} terraces, the behavior in grain boundary regions should be different for two main reasons. First, there are lower average coordination numbers for Au substrate atoms in these regions. In general, this would be expected to weaken the strength of the Au–Au bonds at the surface, relative to those at flat {111} terraces, and thus increase the probability that Au–thiolate complexes could desorb in these low-coordination regions.<sup>65</sup> Indeed, Edinger *et al.* have observed the equivalent of 0.5 monolayer of Au in solution after self-assembly of alkanethiols onto vapor-deposited Au films on Si substrates,<sup>39</sup> surfaces known to contain substantial fractions of grain boundary regions.<sup>18</sup> Second, in the boundary regions, the organization of the chains would be lower than on the {111} terraces. This effect would be expected both to lower the intermolecular barriers to removal of a single chain, thereby accelerating desorption in the defect regions, and to perturb the equilibrium structure of the film, thereby shifting the molecular composition in mixed monolayers. The combination of all these effects would be to prevent the equilibrium structures and compositions on the {111} terraces from dominating those of the total film for all the morphology areas of the gold substrate. Support for such effects is suggested by our data in Table 1 showing the compositional deviation for the 1:3 methyl ester-terminated alkanethiolate SAMs between STM measurements for {111} regions and XPS and IRS measurements averaging the entire surface. While it is not clear what the actual cause of the deviation is, the above discussion does point out complexities which can be introduced into film characteristics by mixed morphology surfaces. In current

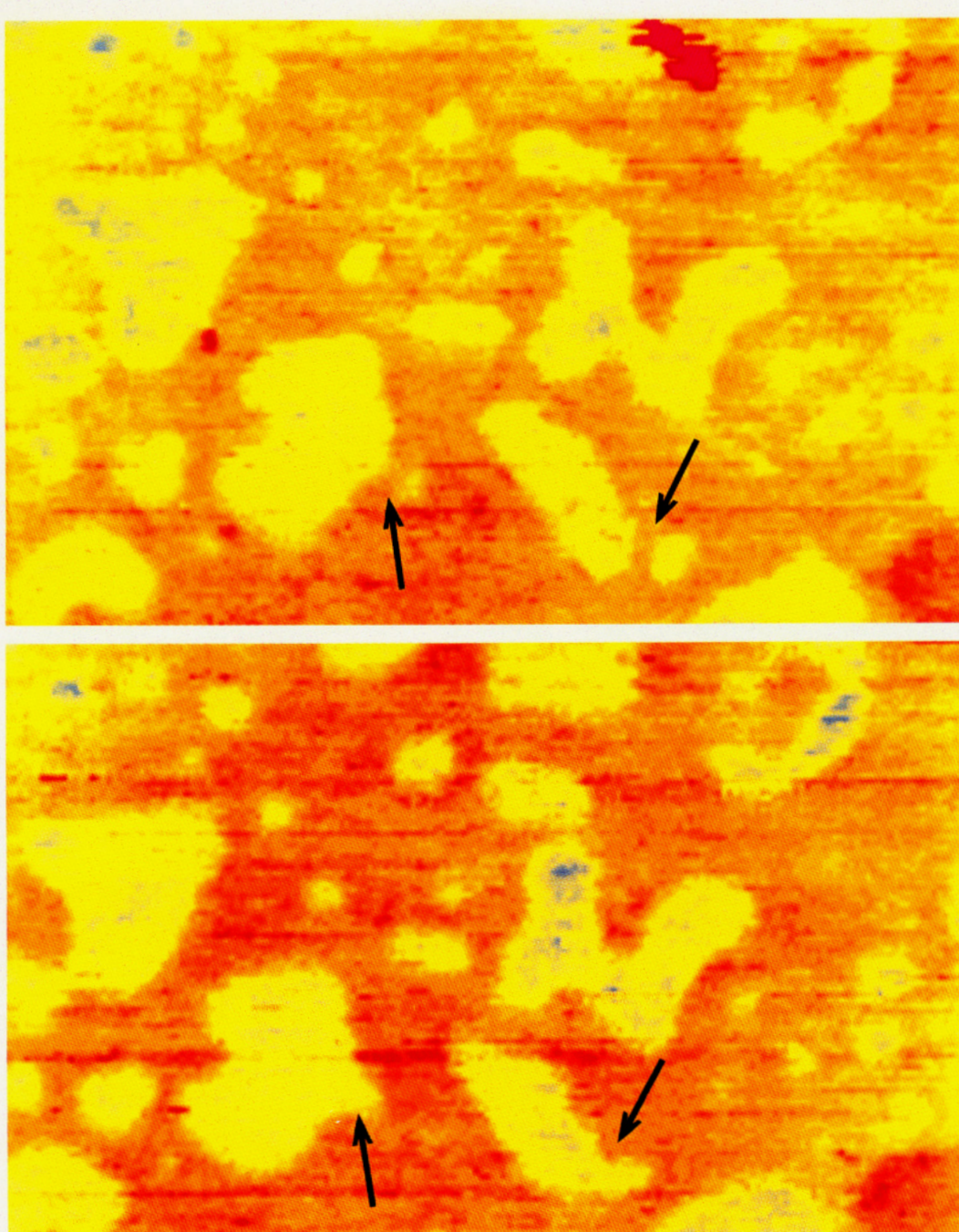


**Figure 9.** Two sequential scanning tunneling microscope images showing a  $500 \times 310 \text{ \AA}^2$  area of a self-assembled monolayer of a mixture of 25%  $\text{CH}_3(\text{CH}_2)_{15}\text{SH}$  and 75%  $\text{CH}_3\text{O}_2\text{C}(\text{CH}_2)_{15}\text{SH}$  on Au. The color scale and tunneling conditions are the same as in Figure 6a. The lower image (b) was recorded 37 min after the upper image (a). Two arrows indicate regions where methyl- and methyl ester-terminated thiolate molecules have exchanged, leading to coalescence of domains of methyl-terminated thiolate molecules.

experiments we are addressing these issues by studying the differences between SAMs deposited on annealed single crystals and on vapor-deposited Au films.

#### IX. Conclusions and Prospects

In summary, we have demonstrated that even weakly interacting molecules which self-assemble can phase separate into discrete molecular domains on the nanometer scale. This calls into question the common assumption that even much more strongly interacting, *i.e.*, hydrogen bonding, molecules randomly mix upon self-assembly. This aspect was never tested previously because the methods used average over much larger surface areas. The application of STM now appears promising as a general probe to characterize nanometer scale phase segregation. This represents an important step in the use of self-assembly techniques in patterned architectures.

We are currently investigating other self-assembled monolayer compositions to determine the generality of the phase segregation observed here. The next critical steps are the determination of the equilibrium surface structures and the unambiguous *chemical* identification of molecular domains via a local spectroscopy. To this end, we are currently performing microwave frequency ac scanning tunneling spectroscopy of these films in order to differentiate and identify the molecules comprising individual domains<sup>66</sup> and experiments in which we image films which have been annealed in order to allow sufficient motion to reach equilibrium surface structures.

**Acknowledgment.** The authors thank Urs Dürig, Sanat Kumar, Ralph Nuzzo, Marc Porter, and Giacinto Scoles for helpful discussions, Sundar Atre for cooperation in obtaining XPS data, and Kyle Krom for help in the preparation of the figures. The

support of the Biotechnology Research and Development Corporation, Hewlett-Packard Company, the National Science Foundation Chemistry, Graduate Research Traineeship and Presidential Young Investigator Programs, and the Office of Naval Research (the above for S.J.S. and P.S.W.) and the National Science Foundation Division of Materials Research (Grant DMR-9001270 for A.N.P. and D.L.A.) is gratefully acknowledged.

## References and Notes

- (1) For example: Fabianowski, W.; Coyle, L. C.; Weber, B. A.; Granata, R. D.; Castner, D. G.; Sadownik, A.; Regen, S. L. *Langmuir* 1989, 5, 35–41. Swalen, J. D.; Allara, D. L.; Andrade, J. D.; Chandross, E. A.; Garoff, S.; Israelachvili, J.; McCarthy, T. J.; Murray, R.; Pease, R. F.; Rabolt, J. F.; Wynne, K. J.; Yu, H. *Langmuir* 1987, 3, 932–950.
- (2) Stenger, D. A.; Georger, J. H.; Dulcey, C. S.; Hickman, J. J.; Rudolph, A. S.; Nielson, T. B.; McCort, S. M.; Calvert, J. M. *J. Am. Chem. Soc.* 1992, 114, 8435–8442. Ertel, S. I.; Ratner, B. D.; Atre, S.; Allara, D. L. Submitted for publication.
- (3) Prime, K. L.; Whitesides, G. M. *Science* 1991, 252, 1164–1167. Frommer, J.; Lüthi, R.; Meyer, E.; Anselmetti, D.; Dreier, M.; Overney, R.; Güntherodt, H.-J.; Fujihara, M. *Nature* 1993, 364, 198.
- (4) Rubinstein, I.; Steinberg, S.; Tor, Y.; Shanzer, A.; Sagiv, J. *Nature* 1988, 332, 426–429. Whitesides, G. M.; Mathias, J. P.; Seto, C. T. *Science* 1991, 254, 1312–1319. Häussling, L.; Ringsdorf, H.; Schmitt, F.-J.; Knoll, W. *Langmuir* 1991, 7, 1837–1840.
- (5) There is precedent for phase segregation in two-dimensional molecular assemblies based on observations of mixed composition Langmuir films formed at the air–water interface.<sup>6,7</sup>
- (6) Birdi, K. S. *Lipid and Biopolymer Monolayers at Liquid Interfaces*; Plenum Press: New York, 1989; pp 107–120.
- (7) Overney, R. M.; Meyer, E.; Frommer, J.; Brodbeck, D.; Lüthi, R.; Howald, L.; Güntherodt, H.-J.; Fujihara, M.; Takano, H.; Gotoh, Y. *Nature* 1992, 359, 133–134.
- (8) Bain, C. D.; Whitesides, G. M. *Science* 1988, 240, 62–63. Bain, C. D.; Whitesides, G. M. *J. Am. Chem. Soc.* 1988, 110, 6560–6561. Bain, C. D.; Whitesides, G. M. *Langmuir* 1989, 5, 1370–1378. Bain, C. D.; Evall, J.; Whitesides, G. M. *J. Am. Chem. Soc.* 1989, 111, 7155–7164. Chidsey, C. E. D.; Bertozi, C. R.; Putvinski, T. M.; Muisce, A. M. *J. Am. Chem. Soc.* 1990, 112, 4301–4306. Ulman, A.; Evans, S. D.; Shnidman, Y.; Sharma, R.; Eilers, J. E.; Chang, J. C. *J. Am. Chem. Soc.* 1991, 113, 1499–1506. Ulman, A.; Evans, S. D.; Shnidman, Y.; Sharma, R.; Eilers, J. E. *Adv. Colloid Interface Sci.* 1992, 39, 175–224.
- (9) Neumann, A. W.; Good, R. J. *J. Colloid Interface Sci.* 1972, 38, 341–358. Schwartz, L. W.; Garoff, S. J. *Colloid Interface Sci.* 1985, 106, 422–437. deGennes, P. G. *Rev. Mod. Phys.* 1985, 57, 827–863.
- (10) Bertilsson, L.; Liedberg, B. *Langmuir* 1993, 9, 141–149.
- (11) Winograd, N. *Anal. Chem.* 1993, 65, 622A–629A.
- (12) We note that large segregated phases in Langmuir films have even been observed optically, by fluorescence microscopy, for a mixture of very dissimilar lipid (dipalmitoylphosphatidylcholine) and cholesterol components. Rice, P. A.; McConnell, H. *Proc. Natl. Acad. Sci. U.S.A.* 1989, 86, 6445–6448.
- (13) Laibinis, P. E.; Nuzzo, R. G.; Whitesides, G. M. *Langmuir* 1992, 8, 1330–1341. Folkers, J. P.; Laibinis, P. E.; Whitesides, G. M. *J. Phys. Chem.* 1992, 96, 5097–5105.
- (14) Siepmann, J. I.; McDonald, I. R. *Mol. Phys.* 1992, 75, 255–259.
- (15) Dubois, L. H.; Nuzzo, R. G. *Annu. Rev. Phys. Chem.* 1992, 43, 437–463 and references therein.
- (16) Nuzzo, R. G.; Dubois, L. H.; Allara, D. L. *J. Am. Chem. Soc.* 1990, 112, 558–569.
- (17) Chidsey, C. E. D.; Loiacono, D. N.; Sleater, T.; Nakahara, S. *Surf. Sci.* 1988, 20, 45–66. Hallmark, V. M.; Chiang, S.; Rabolt, J. F.; Swalen, J. D.; Wilson, R. J. *Phys. Rev. Lett.* 1987, 59, 2879–2882. Widrig, C. A.; Alves, C. A.; Porter, M. D. *J. Am. Chem. Soc.* 1991, 113, 2805–2810.
- (18) Nuzzo, R. G.; Fusco, F. A.; Allara, D. L. *J. Am. Chem. Soc.* 1987, 109, 2358–2367. Troughton, E. B.; Bain, C. D.; Whitesides, G. M.; Nuzzo, R. G.; Allara, D. L.; Porter, M. D. *Langmuir* 1988, 4, 365–385.
- (19) Millipore Purification System, Bedford, MA.
- (20) Laibinis, P. E.; Whitesides, G. M.; Allara, D. L.; Tao, Y.-T.; Parikh, A. N.; Nuzzo, R. G. *J. Am. Chem. Soc.* 1991, 113, 7152–7167.
- (21) Rudolph AutoEL-II, Fairfield, NJ.
- (22) Allara, D. L.; Nuzzo, R. G. *Langmuir* 1987, 1, 45–52.
- (23) Collins, R. W.; Allara, D. L.; Kim, Y.-T.; Shi, J. In *Characterization of Organic Thin Films*; Ulman, A., Ed.; Manning Publications: Greenwich, CT, in press.
- (24) Previous studies have assigned slightly lower values of ~1.45 + 0*i* for densely packed alkyl assemblies (ref 22). An *in-situ* analysis of *n*-alkanethiolate films using spectroscopic ellipsometry from 1.5 to 4.5 eV shows that a value of 1.50 at 632.8 nm yields a better fit to the data.<sup>23</sup>
- (25) Digilab FTS-60, Bio-Rad, Cambridge, MA.
- (26) Buentempo, J. T.; Rice, S. A. *J. Chem. Phys.* 1993, 98, 5835–5840.
- (27) Vig, J. R. *J. Vac. Sci. Technol. A* 1985, 3, 1027–1032.
- (28) UV-Clean, Model UV-C 100, Abtech, Yardley, PA.
- (29) Hewlett-Packard 5950A XPS spectrometer, Palo Alto, CA.
- (30) Folkers, J. P.; Laibinis, P. E.; Whitesides, G. M. *Langmuir* 1992, 8, 1330–1341.
- (31) Besocke, K. *Surf. Sci.* 1987, 181, 145–153. Frohn, J.; Wolf, J. F.; Besocke, K.; Teske, M. *Rev. Sci. Instrum.* 1989, 60, 1200–1201. Stranick, S. J.; Weiss, P. S. *Rev. Sci. Instrum.* 1994, 65, 918–921.
- (32) By measuring the tunneling current vs tip–sample separation in to point contact with the Au substrate,<sup>33</sup> we have shown that the tunneling conditions used correspond to the (nominally Pt–Ir) STM tip being farther from the Au substrate than the outermost portion of the alkanethiolate layer. Dürig *et al.* found for their combination STM/AFM that similar tunneling conditions in ultrahigh vacuum led to their (nominally W) STM tip applying pressure to and thus compressing self-assembled films of the equivalent HO-terminated thiol.<sup>34</sup> We show in the mixed composition studies of section V that we are sensitive to the identity of the outermost functional group of the thiolate. We conclude that the STM tip is not in the thiolate layer but that, under the mild tunneling conditions used, it is unclear whether the STM tip is compressing the thiolate films.
- (33) Gimzewski, J. K.; Möller, R. *Phys. Rev. B* 1987, 36, 1284–1287. Lang, N. D. *Phys. Rev. B* 1987, 36, 8173–8176.
- (34) Dürig, U.; Züger, O.; Michel, B.; Häussling, L.; Ringsdorf, H. *Phys. Rev. B* 1993, 48, 1711–1717.
- (35) Eigler, D. M.; Weiss, P. S.; Schweizer, E. K.; Lang, N. D. *Phys. Rev. Lett.* 1991, 66, 1189–1192. Weiss, P. S.; Eigler, D. M. *Phys. Rev. Lett.* 1993, 71, 3139–3142. Weiss, P. S. *Trends Anal. Chem.* 1994, 13, 61–67.
- (36) Camillone III, N.; Chidsey, C. E. D.; Eisenberger, P.; Fenter, P.; Li, J.; Liang, K. S.; Liu, G.-Y.; Scoles, G. *J. Chem. Phys.* 1993, 99, 744–747.
- (37) Parikh, A. N.; Tao, Y.-T.; Atre, S.; Stranick, S. J.; Weiss, P. S.; Allara, D. L. Manuscript in preparation. Parikh, A. N.; Shi, J.; Lokhore, S.; Nuzzo, R. G.; Allara, D. L. Manuscript in preparation.
- (38) Snyder, R. G.; Hsu, S. L.; Krimm, S. *Spectrochim. Acta, Part A* 1978, 34, 395–406. MacPhail, R. A.; Strauss, H. L.; Snyder, R. G.; Elliger, C. A. *Ibid.* 1984, 88, 334–340. Snyder, R. G.; Strauss, H. L.; Elliger, C. A. *J. Phys. Chem.* 1982, 86, 5145–5150.
- (39) Edinger, K.; Götzhäuser, A.; Demota, K.; Wöll, Ch.; Grunze, M. *Langmuir* 1993, 90, 4–8.
- (40) Kim, Y.-T.; Bard, A. J. *Langmuir* 1992, 8, 1096–1102.
- (41) Chailapakul, O.; Sun, L.; Xu, C.; Crooks, R. M. *J. Am. Chem. Soc.* 1993, 12459–12467.
- (42) McCarley, R. L.; Dunaway, D. J.; Willicut, R. J. *Langmuir* 1993, 9, 2775–2777.
- (43) Schönenberger, C.; Sondag-Huethorst, J. A. M.; Jorritsma, J.; Fokkink, L. G. *J. Langmuir* 1994, 10, 611–614.
- (44) Poirier, G. E.; Tarlov, M. J. *Langmuir*, in press.
- (45) Porter, M. D. Unpublished results.
- (46) Stranick, S. J.; Parikh, A. N.; Allara, D. L.; Weiss, P. S. Manuscript in preparation.
- (47) In the simplest model, the chains are approximated as rigid rods. In this model, for chains tilted at 26–30° and occupying ~21.6 Å<sup>2</sup> per chain (nearest-neighbor spacing of 5.1 Å on a hexagonal lattice),<sup>15,16,20,36</sup> removal of a single chain would produce a depression below the monolayer surface of 12–15 Å (depending upon the tilt azimuth relative to the setting planes in the unit subcell), exposing an adjacent chain. Removal of more than one adjacent chain would expose the substrate. However, at ambient temperature, because thermal energies are significant compared to the CH<sub>2</sub>–CH<sub>2</sub> rotational barriers, chains would be expected to relax conformationally into the molecular void spaces, thereby increasing the defect span while diminishing the depth. Using a model of one missing adsorbate chain in which the first and second ring of surrounding chains (nearest and next-nearest neighbors) are allowed to relax conformationally to an assembly having a slightly lower density (tending toward liquid), we estimate that the 12 chain ensemble would relax to give a 20-Å-diameter hole of 2-Å depth. Thus, we speculate that the smallest observed defects are due to conformational relaxation of no more than a small number of neighboring chains to fill the molecular void left by a single missing chain. The significantly larger defects (in both area and depth) observed by Kim and Bard (ref 40), we then attribute to a much larger number of missing molecules, which even with complete conformational chain relaxation produce hole depths on the scale of the film thickness.
- (48) We note that Dürig *et al.* used shorter incubation periods (20 h) and more dilute solutions ( $3.1 \times 10^{-4}$  M) than those used here.<sup>34</sup> McCarley *et al.* did not report deposition conditions but do observe large defects compared to those reported here.<sup>42</sup>
- (49) The smallest features are difficult to find in the gray scale images. They are visible in Figure 6, repeat from image to image, and are highlighted out in the schematic shown in Figure 6b.
- (50) We have recently observed phase separation for 1:1 mixtures of CH<sub>3</sub>(CH<sub>2</sub>)<sub>15</sub>SH and 25% CH<sub>3</sub>O<sub>2</sub>C(CH<sub>2</sub>)<sub>15</sub>SH on Au[111] as well. These data will be published after further analysis.
- (51) Larger superlattice unit cells for various length alkanethiols self-assembled on Au[111] have recently been observed by a variety of techniques, including He diffraction,<sup>52</sup> X-ray diffraction,<sup>53</sup> low-energy electron diffraction,<sup>54</sup> and STM.<sup>44,45</sup>
- (52) Camillone III, N.; Chidsey, C. E. D.; Liu, G.-Y.; Scoles, G. *J. Chem. Phys.* 1993, 98, 3503–3511.
- (53) Fenter, P.; Eisenberger, P.; Liang, K. S. *Phys. Rev. Lett.* 1993, 70, 2447–2450.

- (54) Dubois, L. H.; Zegarski, B. R.; Nuzzo, R. G. *J. Chem. Phys.* **1993**, *98*, 678–688.
- (55) We are currently performing two-dimensional lattice gas Monte Carlo simulations for reversible mixed adsorption in which the attraction between adsorbate A and adsorbate B is slightly lower than the identical A–A and B–B attractions. The resulting distributions for  $100 \times 100$  lattices of adsorbates after  $10^6$  and more attempted steps per adsorbate show formation of small domains similar in shape and size to images such as those shown in Figures 4–6.
- (56) Folkers, J. P.; Laibinis, P. E.; Whitesides, G. M.; Deutch, J. *J. Phys. Chem.* **1994**, *98*, 563–571.
- (57) Collard, D. M.; Fox, M. A. *Langmuir* **1991**, *7*, 1192–1197. Hickman, J. J.; Ofer, D.; Zou, C.; Wrighton, M. S.; Laibinis, P. E.; Whitesides, G. M. *J. Am. Chem. Soc.* **1991**, *113*, 1128–1132. Wood, M. C.; Atre, S.; Winograd, N.; Allara, D. L. Manuscript in preparation.
- (58) Biebuyck, H. A.; Whitesides, G. M. *Langmuir* **1993**, *9*, 1766–1770.
- (59) Stranick, S. J.; Parikh, A. N.; Allara, D. L.; Weiss, P. S. Submitted for publication.
- (60) In ref 42, McCarley *et al.* have observed motion of the alkanethiolate SAMs driven by the STM tip. In their experiments they initially had larger defects than those reported here which also moved under the influence of the STM tip.<sup>42</sup> The resulting surface after imaging showed steps in the underlying Au substrate with extending “fingers”. No such convoluted step structures are seen in any of our results.
- (61) The barriers to such motions are not known. Sellers *et al.* have recently calculated that, for an isolated thiolate molecule, the barrier to diffusion from 3-fold hollow to 3-fold hollow over the atop site is only 6 kcal/mol<sup>64</sup> compared to the chemisorption energy of ~44 kcal/mol.<sup>15,64</sup>
- (62) Trevor, D. J.; Chidsey, C. E. D.; Loiacono, D. N. *Phys. Rev. Lett.* **1989**, *62*, 929–932. Trevor, D. J.; Chidsey, C. E. D. *J. Vac. Sci. Technol. B* **1991**, *9*, 964–968.
- (63) Peale, D. R.; Cooper, B. H. *J. Vac. Sci. Technol. A* **1992**, *10*, 2210–2215. Cooper, B. H.; Peale, D. R.; McLean, J. G.; Phillips, R.; Chason, E. In *Evolution of Surface and Thin Film Microstructures*; Atwater, H. A., Chason, E., Grabow, M. H., Lagally, M., Eds.; MRS Symposia Proceedings Vol. 280; Materials Research Society: Pittsburgh, 1993; pp 37–46.
- (64) Sellers, H.; Ulman, A.; Shnidman, Y.; Eilers, J. E. *J. Am. Chem. Soc.* **1993**, *115*, 9389–9401.
- (65) TOF-SIMS observations have shown that alkanethiolate species partially desorb from pure SAMs on Au films (vapor-deposited on Si, rougher than the Au on mica films used here) into ethanol solvent and readsorb onto separate pristine Au surfaces also immersed in the solvent. In the presence of a different alkanethiol, slow exchange with the original alkanethiolate species in the film occurs.<sup>57</sup>
- (66) Stranick, S. J.; Weiss, P. S.; Parikh, A. N.; Allara, D. L. *J. Vac. Sci. Technol. A* **1993**, *11*, 739–741. Stranick, S. J.; Weiss, P. S. *J. Phys. Chem.* **1994**, *98*, 1762–1764.